Photon-Assisted Electric Field Domains and Multiphoton-Assisted Tunneling in Semiconductor Superlattices

B. J. Keay,[1] S. J. Allen, Jr.,[1] J. Galán,[2,*] J. P. Kaminski,[1] K. L. Campman,[3] A. C. Gossard,[3] U. Bhattacharya,[4] and M. J. W. Rodwell[4]

[1]*Center for Free-Electron Laser Studies, University of California, Santa Barbara, California 93106*
[2]*Physics Department, The Ohio State University, Columbus, Ohio 43210-1106*
[3]*Materials Department, University of California, Santa Barbara, California 93106*
[4]*Department of Electrical and Computer Engineering, University of California, Santa Barbara, California 93106*

(Received 26 April 1995)

We report the first observation of photon-assisted tunneling induced electric field domains, terahertz multiphoton-assisted tunneling, and an oscillatory dependence of the photon induced currents on terahertz electric field strength in semiconductor superlattices. The new structure in the current-voltage (*I-V*) characteristics as well as the dependence of the current on terahertz electric field strength compares favorably with a model for the current and electrical field profile in superlattices in which new virtual states serve a role similar to the unperturbed quantum well states.

PACS numbers: 73.40.Gk, 72.20.Ht, 73.20.Dx

Photon-assisted tunneling (PAT), long restricted to transport in superconducting junctions [1], has recently emerged in transport in semiconductor superlattices and nanostructures in the presence of high frequency fields [2–4]. The full character of PAT, however, has not been experimentally established.

Electric field inhomogeneities in multiquantum well superlattices have also been studied extensively in the last twenty years [5–8]. Here, we show for the first time that the PAT channels can also support high and low field domains if the terahertz field is strong enough. By using bow-tie antennas we have enhanced the coupling efficiency of terahertz radiation into semiconductor superlattices. This has enabled us to explore PAT induced inhomogeneities as well as multiphoton-assisted tunneling and the terahertz electric field dependence of the PAT channels. An extension of the model of Bonilla *et al.* [8] is put forward that can account in a quantitative way for the detailed *I-V* characteristics of these systems in strong high frequency fields, including both PAT channels and their effect on the electric field domain distribution.

The experiments were performed on a superlattice material consisting of 300 nm of GaAs doped at $n^+ = 2 \times 10^{18}$ cm^{-3}, followed by a 50 nm GaAs spacer layer and ten 33 nm GaAs quantum wells and eleven 4 nm GaAs/$Al_{0.30}Ga_{0.70}As$ barriers and capped by another 50 nm GaAs spacer layer and 300 nm of $n^+ = 2 \times 10^{18}$ cm^{-3} doped GaAs. The substrate was semi-insulating and the superlattice and spacer layers were n doped to 3×10^{15} cm^{-3}. The active area of the superlattice was 8 μm^2. Lithographically defined and processed broadband bow-tie antennas were integrated with the superlattice device and electrically connected to the top and bottom of the superlattice. The devices were then glued onto a high resistivity hemispherical silicon lens (see Fig. 1), and gold wires were bonded to the two gold bows. The experiments were performed over a temperature range of 6–12 K with the sample mounted in a temperature controlled flow cryostat with Z-cut quartz windows. The radiation was incident on the curved part of the Si lens with the polarization parallel to the axis connecting the two gold bows of the bow-tie antenna.

The measured *I-V* characteristic without radiation ($E_{ac} = 0$), dotted line in Fig. 2(c), shows a series of steps in current separated by sawtooth oscillations associated with sequential resonant tunneling in the presence of high and low electric field domains [5–8]. At low bias, the current through the sample occurs via ground state to ground state tunneling. As the bias is increased, the current approaches the critical current, the maximum current that the ground state to ground state tunneling can support, and a quantum well breaks off forming a high field domain. The high field domain is characterized by the alignment of the ground state in one well aligned with the excited state in the "down hill" well. As the bias is increased still further, one well after another breaks off into the high field domain, resulting in the sawtooth, negative differential conductance (NDC) structure, until the entire sample is encompassed by the high field domain. When this occurs the electric field is again uniform and this defines the beginning of a step.

In the presence of the intense terahertz radiation, striking new structure appears in the *I-V* characteristic. The solid line in Fig. 2(c) shows the measured *I-V* characteristic when the superlattice is driven at 3.42 THz. In analogy to our description of the *I-V* characteristic in the absence of the terahertz radiation, the beginning of the new steps correspond to a uniform alignment of the one- or two-photon sidebands, or "virtual" states, associated with the ground state with the third level in the "down hill" well [Fig. 3(a)]. Transport through the ground state

 0031-9007/95/75(22)/4098(4)$06.00

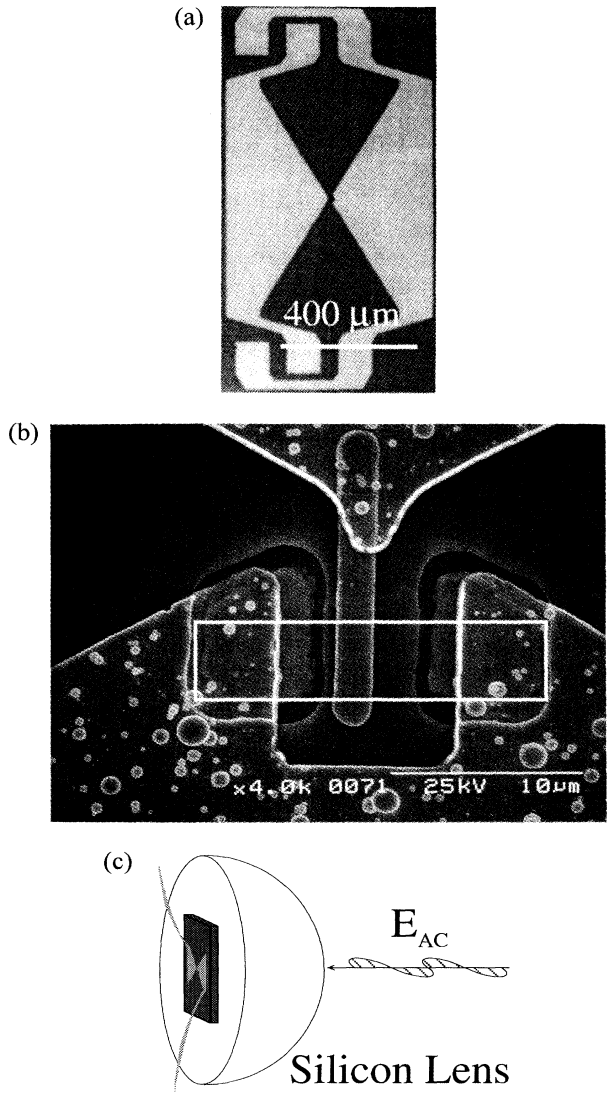

FIG. 1. (a) An optical photograph of the bow-tie antenna coupled superlattice. (b) A scanning electron microscope of a bow-tie antenna coupled superlattice where the white box illustrates the area protected during ion implantation. (c) An illustration of the bow-tie antenna mounted on a hemispherical silicon lens.

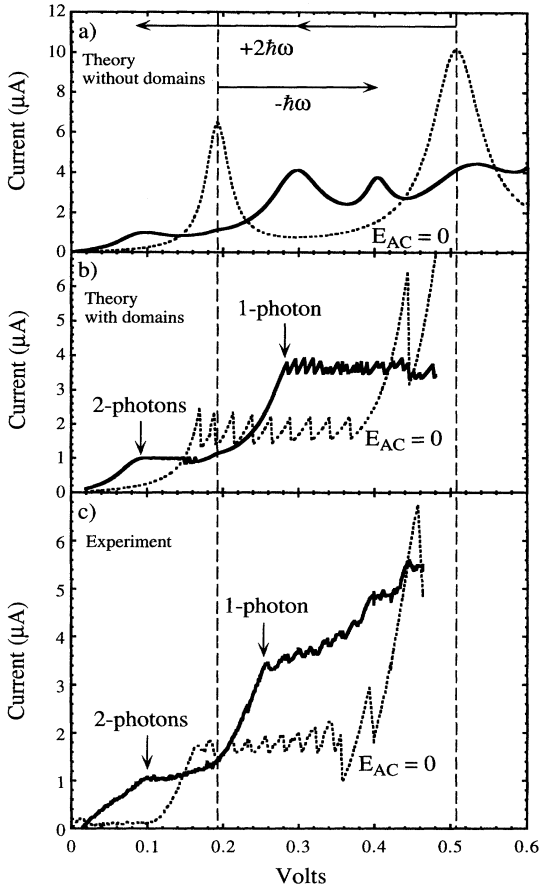

FIG. 2. The current-voltage characteristics of a superlattice with 3.42 THz radiation (solid lines) and without terahertz radiation (dotted lines): (a) The calculated *I-V* of the superlattice without electric field domains, (b) the calculated *I-V* characteristic with electric field domains, and (c) the measured *I-V*.

(zero photons) and the structure associated with the *I-V* without radiation has been suppressed.

Remarkably, the sawtooth NDC structure observed on the one-photon step is similar to the structure in the *I-V* characteristic without terahertz radiation. This implies that on the plateau associated with the PAT step the superlattice supports high and low electric field domains, but sustained by the PAT channels. That is to say, transport occurs via tunneling between the one-photon virtual state associated with the ground state, and the third energy level in the low field domain and via the real ground state and the third energy level tunneling in the high field domain [Fig. 3(b)].

To theoretically model the behavior described here, we have extended the model introduced by Bonilla *et al.* [8]. The key assumption in that model is the existence of a tunneling probability between neighboring quantum wells in the presence of an external electric field that exhibits a region of NDC. The origin of this NDC is physically very clear, alignment and misalignment of subband states in an applied dc electric field (E_{dc}).

Following Tien and Gordon [1], the action of the high frequency field is included by introducing new quantum well virtual states separated from the unperturbed ground state by $\pm n\hbar\omega$ (Fig. 3), with a state density proportional to $J_n^2(edE_{ac}/\hbar\omega)$, where J_n is the nth order Bessel function, d is the superlattice period, E_{ac} is the magnitude of the terahertz electric field, and $\hbar\omega$ is the photon energy. In this model these new virtual states appear only in the well from which the electron tunnels. The tunneling

probability is enhanced whenever the resonance condition is fulfilled and given by

$$P(V_{dc}, E_{ac}, \omega) = \sum_{j=2}^{4} \sum_{n=-\infty}^{\infty} J_n^2\left(\frac{edE_{ac}}{\hbar\omega}\right) T_{1j} \Lambda(n\hbar\omega + eV_{dc} + E_1 - E_j), \quad (1)$$

where T_{1j} is the square of the overlap integral, E_j are energies of the jth state in the well without the external fields, and the $\Lambda(n\hbar\omega + eV_{dc} + E_1 - E_j)$ are Lorentzians [8].

In Fig. 2(a) we show the calculated I-V characteristic for a uniform electric field (no domains) with 3.42 THz radiation ($E_{ac} = 7$ kV/cm) compared with the result in absence of external radiation ($E_{ac} = 0$). The length of the arrows indicates the energy of the photon times the number of wells and identifies the location of the new PAT resonances. The different PAT peaks are the resonances that come from the net "emission" (negative n) or net "absorption" (positive n), of n-photons.

It is important to note that the terahertz currents induced in the superlattice may be rich in harmonics. However, the device impedance is very large, and the harmonic currents do not alter the field at the vertex of the antenna. As a result, the terahertz voltage and electric fields will essentially contain only the fundamental frequency, and we are not concerned with multiphoton features caused by harmonics of the applied THz field.

The calculated current-voltage characteristic, with electric field domains, is shown in Fig. 2(b) and compares well with the experimental results [Fig. 2(c)]. By comparing the calculation without domains [Fig. 2(a)] and the calculation with domains [Fig. 2(b)], we immediately learn several important things. First, the system may jump to the domain solution before reaching the maximum tunneling probability. Second, the emission process that is apparent in the tunneling probability [Eq. (1)] and Fig. 2(a) is obscured in the modeled current voltage characteristics that include electric field domains. There are two reasons for this: The tunneling probability accompanied by emission $\propto T_{12}$ is less than the tunneling probability accompanied by absorption to the next higher level $\propto T_{13}$ and once the electric field domain structure is formed the system does not change branch until the next important peak in the tunneling probability is reached. The emission process has not appeared in a convincing manner and this may offer an explanation.

Figure 4 shows the PAT step location in voltage, induced in the I-V characteristic by the terahertz radiation, as a function of the laser frequency. The step edge is located by the minimum of $\partial^2 I/\partial V^2$ of the I-V's. The dotted lines are interpolations between the $\omega = 0$ intercept on the voltage axis, the voltage at which the step occurs in the absence of a terahertz field, and the zero voltage intercept on the frequency axis, which we expect at $n\hbar\omega = E_3 - E_1 = 32.7$ meV (7.9 THz), or $E_2 - E_1 = 12.4$ meV (3.0 THz). Here n is $1, 2, 3, \ldots$ as the PAT process involves $1, 2, 3, \ldots$ photons and the energy levels are calculated in the envelope function approximation. By

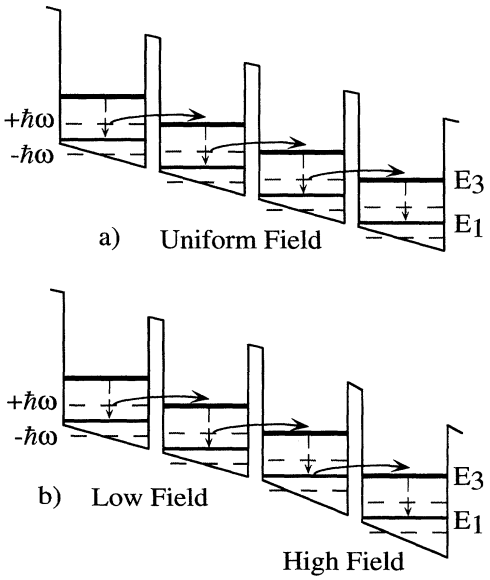

FIG. 3. The energy level diagram, with $\pm\hbar\omega$-photon sidebands, showing the state alignment corresponding to (a) the one-photon step edge in Fig. 2(c) (uniform electric field) and (b) the electric field domain structure on the one-photon step in Fig. 2(c). The second energy level (E_2) and the $\pm 2\hbar\omega$ sidebands are not shown for clarity.

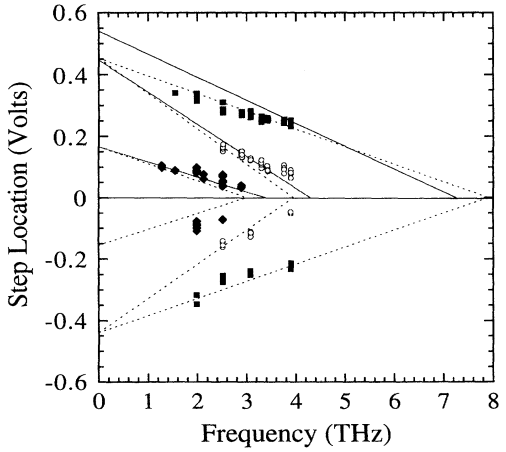

FIG. 4. The step location in volts vs frequency. The data points correspond to the $E_1 \rightarrow E_3$, one-photon transition (solid squares), the $E_1 \rightarrow E_3$, two-photon transition (open circles), and the $E_1 \rightarrow E_2$, one-photon transition (solid diamonds). The dotted lines are obtained from the simple linear dependence on dc electric field described in the text. The solid lines are obtained from the model calculation.

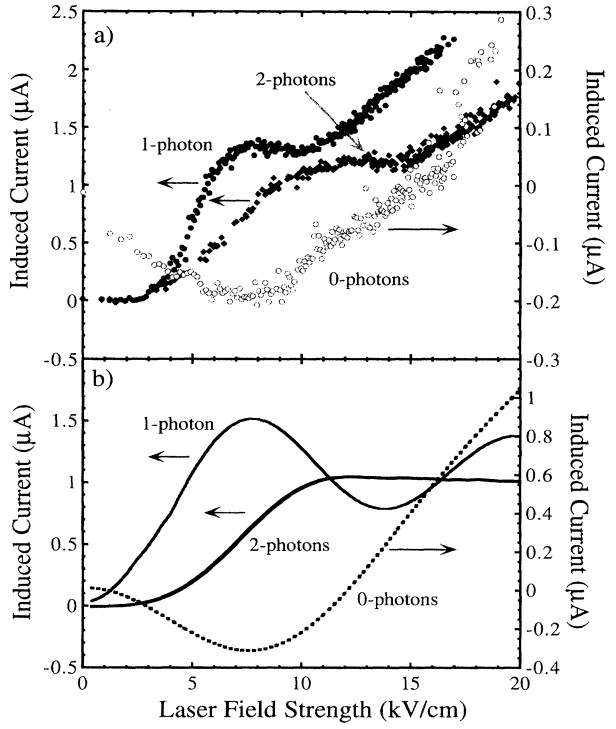

FIG. 5. (a) The induced current vs laser field strength at bias points sensitive to the indicated multiphoton processes. (b) The induced current obtained from the simulation.

using the domain model we generate the solid lines in Fig. 4.

The distinguishing prediction of the model of Tien and Gordon [1] is that the strength of the PAT channels is expected to exhibit nonmonotonic dependence on the terahertz electric field strength. In particular, since the occupancy of the virtual states is proportional to J_n^2, the induced current through virtual states should also be proportional to J_n^2. To test this idea we have displayed the induced current as a function of laser field strength [Fig. 5(a)], measured with sample in the 3.42 THz radiation, at three key bias points of the *I-V* shown in Fig. 2(c), corresponding to transport through the ground state (zero photons) 5 mV through the two-photon virtual state (100 mV) and through the one-photon virtual state (250 mV). In Fig. 5(a) we have scaled the electric field axis so that the local maximum for the one-photon and two-photon processes and the local minimum for the zero-photon process are best fit to the appropriate maxima, or minima, of J_n^2. With this scaling, the nonmonotonic dependence is seen to be consistent with the model of Tien and Gordon.

In Fig. 5(b) we show the induced current at the multiphoton-assisted features, derived from the domain model. The agreement with experiment is satisfactory. The nonmonotonic dependence on terahertz electric field strength is a vestige of the oscillatory behavior described above, but the simple Bessel function-like behavior is not observed and not expected due to the complex nature of the *I-V* characteristic in the presence of domains and multiphoton channels. It should be pointed out that the modeled zero-photon current (dotted line) was calculated at the first static resonance (190 mV) instead of at 5 mV, since the model does not include miniband transport.

In conclusion, we report the first observation of electric field domain structure defined by tunneling between virtual states and the real quantum well states as well as multiphoton-assisted tunneling and a nonmonotonic dependence of the multiphoton-assisted tunneling induced currents on terahertz field strength in semiconductor multiquantum well superlattices. We have successfully extended a recent model for current voltage characteristics of sequential resonant tunneling superlattices in the presence of electric field domains by inserting new subband states in the spirit of Tien and Gordon [1].

We would like to thank the staff at the Center for Free-Electron Laser Studies, J. R. Allen, D. Enyeart, J. P. Kaminski, G. Ramian, and D. White. The Center for Free-Electron Laser Studies is supported by the Office of Naval Research. Funding for this project was provided by the Army Research Office, the NSF, and the Air Force Office of Scientific Research. J. G. wishes to acknowledge financial support from MEC-Fulbright ONR.

*Permanent address: Universidad Carlos III Madrid. Leganés 28911, Spain.

[1] P. K. Tien and J. P. Gordon, Phys. Rev. **129**, 647 (1963).
[2] P. S. S. Guimaraes, B. J. Keay, J. P. Kaminski, S. J. Allen, Jr., P. F. Hopkins, A. C. Gossard, L. T. Florez, and J. P. Harbison, Phys. Rev. Lett. **70**, 3792 (1993).
[3] L. P. Kouwenhoven, S. Jauhar, J. Orenstein, P. L. McEuen, Y. Nagamune, J. Motohisa, and H. Sakaki, Phys. Rev. Lett. **73**, 3443 (1994).
[4] J. Faist, F. Capasso, D. L. Sivco, C. Sirtori, A. L. Hutchinson, and A. Y. Cho, Science **264**, 553–556 (1994).
[5] L. Esaki and L. L. Chang, Phys. Rev. Lett. **33**, 495 (1974).
[6] K. K. Choi, B. F. Levine, R. J. Malik, J. Walker, and C. G. Bethea, Phys. Rev. B **35**, 4172 (1987).
[7] H. T. Grahn, R. J. Haug, W. Müller, and K. Ploog, Phys. Rev. Lett. **67**, 1618 (1991).
[8] L. L. Bonilla, J. Galán, J. A. Cuesta, F. C. Martínez, and J. M. Molera, Phys. Rev. B **50**, 8644 (1994).

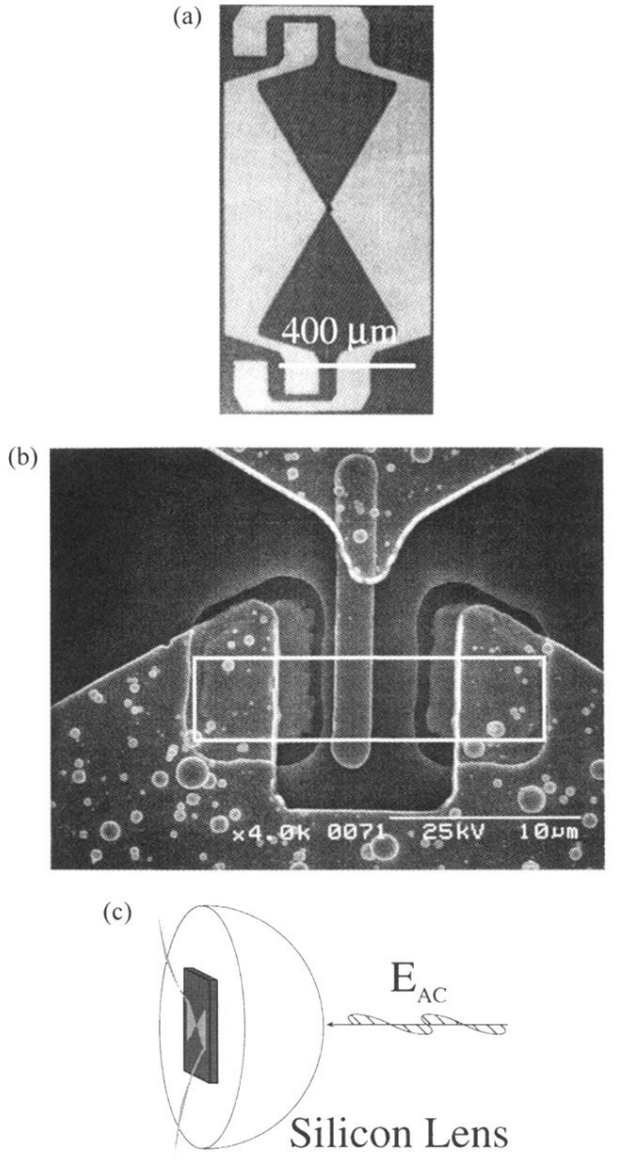

FIG. 1. (a) An optical photograph of the bow-tie antenna coupled superlattice. (b) A scanning electron microscope of a bow-tie antenna coupled superlattice where the white box illustrates the area protected during ion implantation. (c) An illustration of the bow-tie antenna mounted on a hemispherical silicon lens.